SOIL RESPIRATION

Soil respiration–driven CO_2 pulses dominate Australia's flux variability

Eva-Marie Metz[1]*, Sanam N. Vardag[1,2], Sourish Basu[3,4], Martin Jung[5], Bernhard Ahrens[5], Tarek El-Madany[5], Stephen Sitch[6], Vivek K. Arora[7], Peter R. Briggs[8], Pierre Friedlingstein[9,10], Daniel S. Goll[11], Atul K. Jain[12], Etsushi Kato[13], Danica Lombardozzi[14], Julia E. M. S. Nabel[5,15], Benjamin Poulter[16], Roland Séférian[17], Hanqin Tian[18], Andrew Wiltshire[19], Wenping Yuan[20], Xu Yue[21], Sönke Zaehle[5], Nicholas M. Deutscher[22], David W. T. Griffith[22], André Butz[1,2,23]*

The Australian continent contributes substantially to the year-to-year variability of the global terrestrial carbon dioxide (CO_2) sink. However, the scarcity of in situ observations in remote areas prevents the deciphering of processes that force the CO_2 flux variability. In this study, by examining atmospheric CO_2 measurements from satellites in the period 2009–2018, we find recurrent end-of-dry-season CO_2 pulses over the Australian continent. These pulses largely control the year-to-year variability of Australia's CO_2 balance. They cause two to three times larger seasonal variations compared with previous top-down inversions and bottom-up estimates. The pulses occur shortly after the onset of rainfall and are driven by enhanced soil respiration preceding photosynthetic uptake in Australia's semiarid regions. The suggested continental-scale relevance of soil-rewetting processes has substantial implications for our understanding and modeling of global climate–carbon cycle feedbacks.

Terrestrial ecosystems drive the seasonal and year-to-year variability of the global carbon dioxide (CO_2) sink (*1*). Previous research has identified semiarid regions as hotspots of global CO_2 balance interannual variability (*2*–*5*) because of the strong sensitivity of photosynthetic carbon uptake to fluctuations in water availability (*6*, *7*). The Australian continent is primarily covered with semiarid ecosystems and experiences large variations in rainfall. These conditions make Australia particularly relevant for the variability in the global carbon cycle (*8*–*13*), contributing up to 60% of yearly anomalies in the global terrestrial CO_2 sink (*2*).

However, attribution of global CO_2 sink variations to certain regions and mechanisms is highly uncertain, which limits our ability to model climate–carbon cycle feedbacks and project future climate (*14*, *15*). Global process-based ecosystem models underestimate observed CO_2 flux variability across semiarid sites owing to the complexity of carbon–water cycle interactions and the diversity of ecosystem responses to water fluctuations (*16*, *17*). The same holds true for machine learning–based models trained on local carbon flux observations (*18*, *19*) given the scarcity of available flux measurements in low-latitude semiarid regions (*20*) and the inability to represent potentially important noninstantaneous carry-over effects (*21*). Atmospheric transport inversions based on in situ measurements of airborne CO_2 also suffer from the scarcity of observations in remote areas, and therefore the inversions cannot reliably attribute CO_2 flux variability to specific regions, despite growing monitoring capacities (*22*, *23*). However, recent satellite observations of atmospheric column CO_2 deliver data where ground-based in situ concentration measurements and carbon flux networks are sparse, and thus, satellite CO_2 data can fill important gaps and provide new constraints on regional-scale patterns and processes (*8*, *24*–*28*).

In this study, using satellite observations of atmospheric CO_2 concentrations from the Greenhouse Gases Observing Satellite (GOSAT) for the period 2009–2018, we identify a net CO_2 pulse to the atmosphere of variable magnitude that occurs over Australia at the end of the dry season in most years. We show that this pattern—which is not evident in traditional atmospheric inversions using in situ measurements only, in the FLUXCOM machine learning–based extrapolations of in situ flux measurements (*18*, *20*), or in most process-based ecosystem models of the TRENDY initiative (*29*)—appears to dominate the seasonal and year-to-year variations of Australia's CO_2 balance for that period. The few process-based TRENDY models that reproduce the CO_2 pulse pattern qualitatively suggest that it is caused by rapid respiratory carbon release with the onset of the rainy season while the increase in photosynthetic carbon uptake lags behind. This observed process is consistent with the phenomenon of respiration pulses after rewetting events discussed in the context of the "Birch effect" (*30*, *31*). Such pulses have been described extensively in local studies of water-limited systems (*32*), but their large-scale relevance has remained unknown.

Atmospheric CO_2 peak over Australia

The GOSAT has been delivering global measurements of the column-average dry-air mole fractions ("concentrations") of atmospheric CO_2 since its launch in 2009 (*33*). After subtracting the secular trend (*34*), the record of GOSAT concentrations for the period 2009–2018 (Fig. 1) reveals a seasonal pattern above Australia with CO_2 drawdown in March, April, and May (MAM) and a CO_2 peak of variable magnitude at the end of the dry season in October, November, and December (OND). These patterns are consistent among two retrievals independently applied to GOSAT [GOSAT/RemoTeC (*35*) and GOSAT/ACOS (*36*); table S1], and they are present in CO_2 concentrations measured by the Orbiting Carbon Observatory-2 [OCO-2 (*37*, *38*), period 2015–2018; table S1) as well as in ground-based data of the Total Carbon Column Observing Network (TCCON) (*39*) (figs. S1 and S2).

In contrast, the atmospheric column CO_2 concentrations simulated by three inverse atmospheric transport models—CarbonTracker CT2019B (*40*), CAMS (*41*), and TM5-4DVAR (*42*)—underestimate the CO_2 drawdown in MAM and lack the CO_2 pulses in OND (Fig. 1). Driven by atmospheric wind data, these transport models deliver concentration fields that are optimally compatible with in situ–measured CO_2 concentrations and the a priori biogenic, oceanic, fire, and fossil CO_2 surface-atmosphere fluxes (*34*). However, given their sparsity in

[1]Institute of Environmental Physics, Heidelberg University, 69120 Heidelberg, Germany. [2]Heidelberg Center for the Environment (HCE), Heidelberg University, 69120 Heidelberg, Germany. [3]Goddard Space Flight Center, NASA, Greenbelt, MD 20771, USA. [4]Earth System Science Interdisciplinary Center, University of Maryland, College Park, MD 20740, USA. [5]Max Planck Institute for Biogeochemistry, 07745 Jena, Germany. [6]College of Life and Environmental Sciences, University of Exeter, Exeter EX4 4RJ, Devon, UK. [7]Canadian Centre for Climate Modelling and Analysis, Environment and Climate Change Canada, Victoria, BC V8N 1V9, Canada. [8]Climate Science Centre, CSIRO Oceans and Atmosphere, Canberra, ACT 2601, Australia. [9]College of Engineering, Mathematics and Physical Sciences, University of Exeter, Exeter EX4 4QF, UK. [10]Laboratoire de Météorologie Dynamique, Institut Pierre-Simon Laplace, CNRS-ENS-UPMC-X, Département de Géosciences, Ecole Normale Supérieure, 75005 Paris, France. [11]Université Paris Saclay, CEA-CNRS-UVSQ, LSCE/IPSL, 91191 Gif sur Yvette, France. [12]Department of Atmospheric Sciences, University of Illinois Urbana-Champaign, Urbana, IL 61801, USA. [13]Institute of Applied Energy, Tokyo 105-0003, Japan. [14]Climate and Global Dynamics Laboratory, National Center for Atmospheric Research, Boulder, CO 80305, USA. [15]Max Planck Institute for Meteorology, 20146 Hamburg, Germany. [16]Biospheric Sciences Laboratory, Goddard Space Flight Center, NASA, Greenbelt, MD 20771, USA. [17]CNRM, Université de Toulouse, Météo-France, CNRS, 31057 Toulouse, France. [18]Schiller Institute for Integrated Science and Society, Department of Earth and Environmental Sciences, Boston College, Chestnut Hill, MA 02467, USA. [19]Met Office Hadley Centre for Climate Science and Services, Exeter EX1 3PB, UK. [20]School of Atmospheric Sciences, Southern Marine Science and Engineering Guangdong Laboratory (Zhuhai), Sun Yat-sen University, Zhuhai 519082, China. [21]Jiangsu Key Laboratory of Atmospheric Environment Monitoring and Pollution Control, Jiangsu Collaborative Innovation Center of Atmospheric Environment and Equipment Technology, School of Environmental Science and Engineering, Nanjing University of Information Science and Technology (NUIST), Nanjing 210044, China. [22]Centre for Atmospheric Chemistry, School of Earth, Atmospheric and Life Sciences, University of Wollongong, Wollongong, NSW 2522, Australia. [23]Interdisciplinary Center for Scientific Computing (IWR), Heidelberg University, 69120 Heidelberg, Germany.
*Corresponding author. Email: eva-marie.metz@iup.uni-heidelberg.de (E.-M.M.); andre.butz@iup.uni-heidelberg.de (A.B.)

and around Australia (compare fig. S3 and fig. S4), the in situ measurements provide only marginal constraints on the regional flux balance. Thus, the discrepancy between CO_2 concentrations from GOSAT and traditional in situ–based atmospheric inversions hints at the existence of a carbon release mechanism in Australian ecosystems that has remained undetected by the existing in situ CO_2 monitoring system.

Australian top-down and bottom-up fluxes

To improve upon the surface flux estimates for Australia, we fed the GOSAT CO_2 concentrations into one of the atmospheric inverse models (TM5-4DVAR) together with the in situ CO_2 measurements. We find that the recurring end-of-dry-season CO_2 concentration peaks are indeed attributed to a carbon release pattern originating from land ecosystems, which is not present in the inversions when assimilating in situ CO_2 data alone (Fig. 2A and fig. S5).

Our new estimates of Australia's carbon balance variability based on assimilating GOSAT together with in situ data show a nearly doubled peak-to-peak amplitude of the seasonal cycle (175 ± 40 TgC/month, mean ± standard deviation over the 2009–2018 period, July-to-June peak-to-peak amplitude) compared with the in situ–only inversions (88 ± 13 TgC/month). Moreover, the end-of-dry-season CO_2 pulses found by the GOSAT inversions imply a more than fourfold greater year-to-year variability of the annual CO_2 fluxes (0.207 PgC/year, standard deviation over the 2010–2018 period) than for the in situ–only inversions (0.039 PgC/year) (fig. S6 and table S2). Fluxes obtained by assimilating OCO-2 together with in situ data for the period 2015–2018 show the same end-of-dry-season pulses and agree well with the fluxes of the GOSAT inversion (fig. S7).

To understand the origin of the CO_2 pulses, we compared the top-down inversions with bottom-up estimates from machine learning [FLUXCOM (*18*, *20*)] and 18 process-based dynamic global vegetation models (DGVMs) from the TRENDY (v9) ensemble (*42*). The DGVMs also provide the component fluxes of gross primary productivity (GPP) and terrestrial ecosystem respiration (TER) enabling the attribution to variations in photosynthetic carbon uptake and respiratory carbon release. We further included fire emissions (FIRE) from the Global Fire Emission Database (GFED) as a potential factor for explaining the pattern. To compare with the top-down inversions, we calculated net biome production (NBP = TER + FIRE − GPP) by adding fire emissions from GFED to net ecosystem exchange (NEE = TER − GPP) from FLUXCOM. With this sign convention, positive fluxes correspond to carbon emissions into the atmosphere. For TRENDY, NBP was taken directly from the simulations of the DGVMs. We find that FLUXCOM+GFED–derived NBP lacks the end-of-dry-season CO_2 pulses (Fig. 2A), and its seasonal amplitude (64 ± 16 TgC/month) underestimates the one found by the GOSAT inversions by a factor of three. This could be explained by the sparsity of Australian flux tower data in the training of the FLUXCOM machine learning models (only 4 of 224 sites are located in Australia; see fig. S3), causing extrapolation errors (*18*), and by known weaknesses in representing certain fluctuations in response to water availability (*19*) or "memory" effects due to unaccounted carbon pool dynamics (*43*). Our analysis further suggests that local and transported fire emissions might contribute at the beginning of the

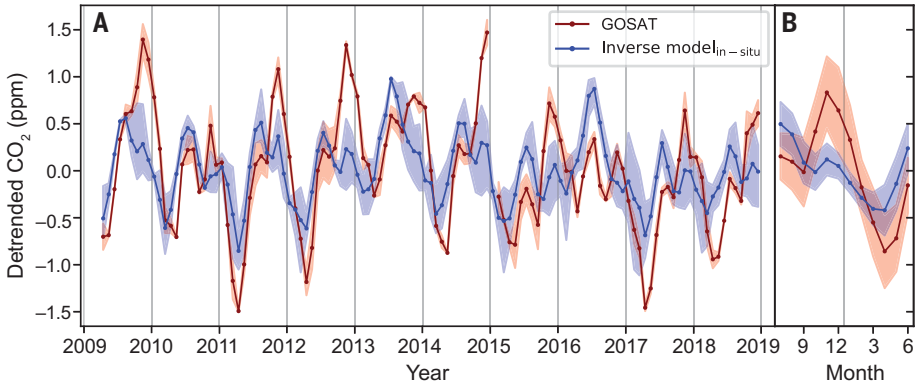

Fig. 1. Detrended CO_2 concentrations over Australia from satellite and models. (**A**) Detrended column-average dry-air mole fractions of CO_2 measured by GOSAT (red) and simulated by inverse models assimilating in situ ground-based measurements (blue). Data are monthly averages for Australia. Red shading indicates the range of the GOSAT/RemoTeC and GOSAT/ACOS algorithms. Blue shading indicates the range of the CarbonTracker, CAMS, and TM5-4DVAR inverse models. ppm, parts per million. (**B**) Mean and standard deviation (shading) over the period 2009–2018.

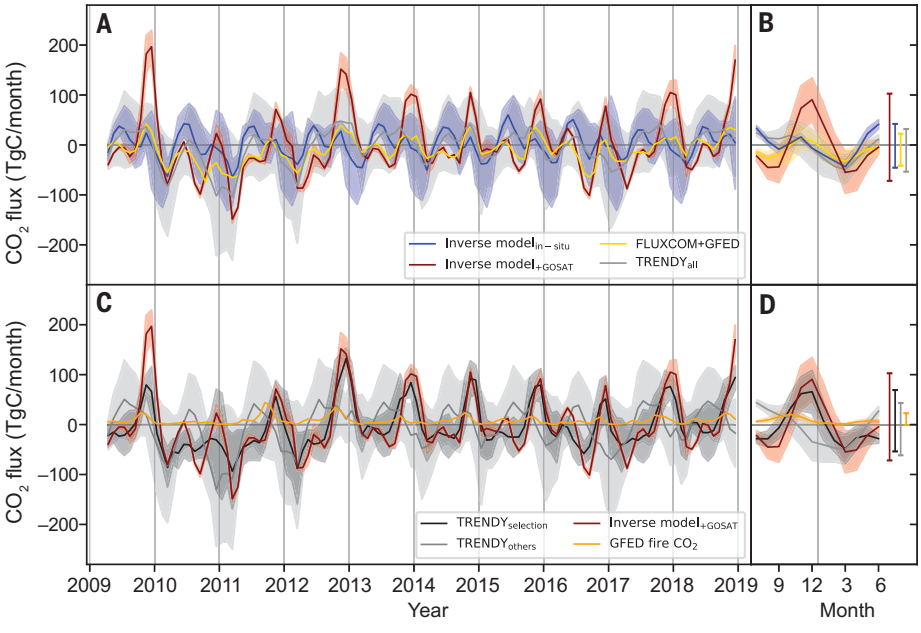

Fig. 2. Australian net CO_2 fluxes. (**A**) Top-down estimates of the net monthly Australian CO_2 fluxes inferred by in situ CO_2 measurement–based inverse models (blue) and by TM5-4DVAR assimilating in situ measurements together with GOSAT observations (red), compared with bottom-up FLUXCOM+GFED NBP (yellow) and the TRENDY ensemble mean NBP (gray). Shading indicates the range among the various top-down data streams (in situ–based CarbonTracker, CAMS, and TM5-4DVAR in blue, TM5-4DVAR$_{+GOSAT/RemoTeC}$ and TM5-4DVAR$_{+GOSAT/ACOS}$ in red) and the standard deviation among the TRENDY ensemble (gray). (**C**) NBP of a subgroup of TRENDY models (black) compared with the other models (gray), with the GOSAT inversions [red, same as in (A)], and with GFED fire emissions (orange). Shading as in (A). (**B** and **D**) Mean and standard deviation (shading) over the period 2009–2018 and the mean peak-to-peak seasonal cycle amplitudes (bars). Positive fluxes correspond to carbon emissions into the atmosphere.

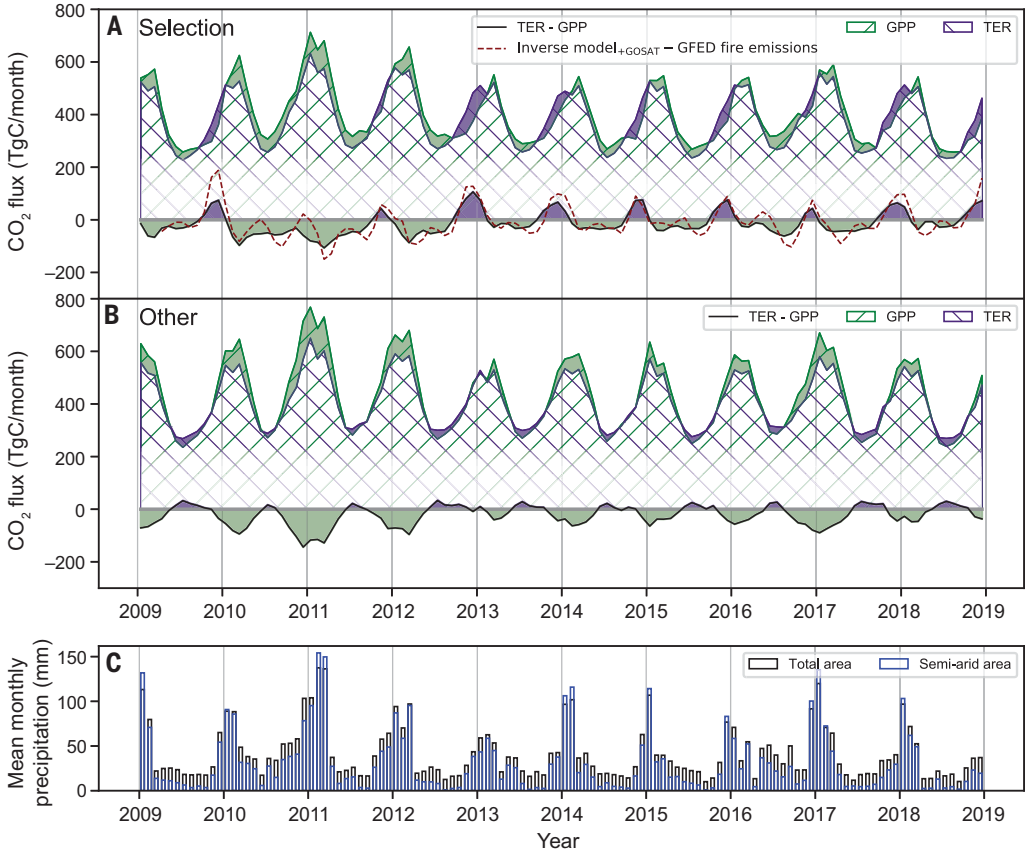

Fig. 3. Seasonal timing of gross CO_2 fluxes among TRENDY models. (**A**) Gross primary production (GPP, green) and total respiration (TER, purple) for Australia for the selection of TRENDY DGVMs that replicate the end-of-dry-season CO_2 pulses. The difference of TER and GPP is given in black in the lower part together with GOSAT-based inversion where GFED fire emissions are subtracted (dashed red line). (**B**) Same as (A), but for the other TRENDY models that do not replicate the end-of-dry-season CO_2 pulses. (**C**) Mean monthly precipitation over the entire Australian region (black) and the semiarid part (fig. S3) of Australia (blue).

carbon pulses but cannot explain their magnitude and duration (Fig. 2B and fig. S8).

The ensemble of TRENDY NBP simulations shows a large intermodel spread and also no end-of-dry-season CO_2 pulses on average (Fig. 2A) causing a seasonal amplitude (85 ± 20 TgC/month) that is about half of that of the GOSAT inversions. However, the dry season pulses are present in a subset of five of the TRENDY DGVMs [Fig. 2B and table S1; "Characteristics of $TRENDY_{selection}$" in (*34*)]. For this subset, the timing, duration, and magnitude (except for the year 2009) of the pulses and their seasonal amplitude (123 ± 31 TgC/month) are closer to the pulses found by the GOSAT inversions. This finding suggests that the CO_2 pulses can be explained by ecosystem processes shaping the phasing of photosynthesis and respiration.

Phasing of respiration and photosynthesis

We find that the subset of DGVMs that are in good agreement with the GOSAT inversions reveal a distinctly different seasonal timing of GPP and TER than the other DGVMs. For the selected subset, the CO_2 pulses are driven by TER, which increases rapidly at the onset of the rainy season, whereas GPP picks up only a few weeks later (Fig. 3A). The pulses originate mainly from an early increase of soil respiration in semiarid regions (figs. S9 and S10A). For the other DGMVs, TER and GPP show a mostly synchronous phasing throughout the year, yielding no CO_2 pulses (Fig. 3B and fig. S10B). The precipitation records for the semiarid regions of Australia (Fig. 3C and fig. S3) suggest that the soil respiration–driven pulses shown by the GOSAT inversions and the selected TRENDY models are weaker or do not occur in years with anomalously strong precipitation during the dry period (Austral winter), such as in the La Niña years 2010 and 2016. This implies that the observed pulses are conditional on rewetting of dry soils and that it is through the strength of the pulses that climatic conditions exert control over Australia's annual CO_2 balance (fig. S6).

The detected continental-scale CO_2 pulses are consistent with site-level observations of dryland ecosystems that show an asynchronous response of respiration and photosynthesis to precipitation pulses (*44*). The rapid response of microbial respiration to rewetting events is known as the "Birch effect" and has been described in the literature of specific sites in some semiarid regions for many decades (*30*–*32*). After being dormant in the dry period, soil microbes are activated by the moisture supply from rainfall. Under warm soil temperatures, the microbes quickly respire accumulated and readily available substrate and their populations grow rapidly. These dynamics of soil microbial processes cause respiration CO_2 pulses with rewetting of dry soils that are evident in Australian flux tower data (figs. S11 and S12). Photodegradation of surface litter (*45*) and the death of microorganisms during the dry period (*46*, *47*) may lead to the accumulation of easily decomposable substrate available to microorganisms at the onset of rain. It remains an open question whether the respiration pulses are mainly driven by substrates accumulated during the dry period and to what extent they are fueled by mobilization and decomposition of physically protected carbon (*47*). These processes are not represented explicitly or in detail in the TRENDY DGVMs, and thus the DGVMs cannot resolve how the site-level mechanisms scale up to the continental-scale effect observed here. Nonetheless, a selection of models effectively captures the continental-scale CO_2 pulses by a fast response of respiration and a delayed response of photosynthesis to the onset of the rainy season. This highlights the importance of subtle differences in effective parameterizations of respiration and photosynthesis to moisture fluctuations. Associated uncertainties affect the ability of the models to accurately represent the carbon cycle of semiarid ecosystems.

Our study demonstrates that the soil respiration–driven CO_2 pulses over Australia after the end of the dry season are of large-scale relevance and appear to dominate the variability of the continent's carbon balance.

The GOSAT inversions have shed light on a blind spot of previous top-down and bottom-up approaches for quantifying and attributing CO_2 flux variability. This is important because Australia's semiarid regions contribute substantially to the interannual variability of the global terrestrial carbon sink and because it is the ecosystem response to the phasing of dry and wet periods that drives the seasonal mechanism behind the large interannual variability. Thus, our study calls for revisiting the contributions of global semiarid systems to CO_2 balance variations and for assessing implications for our ability to model climate-carbon feedbacks in semiarid regions. Only a few of the global vegetation models are able to reproduce the observed CO_2 pulses, which suggests that only their respective parameterizations are able to represent the sensitivity of the underlying mechanism to changes in climatic conditions and, thus, to accurately project semiarid CO_2 flux variability under a changing climate. Considering the large uncertainties associated with modeling climate-carbon feedbacks (*14*, *15*, *48*), our findings may contribute continental-scale mechanistic understanding that can help reduce these uncertainties for dryland ecosystems that are found to be particularly sensitive to climate change (*49*).

REFERENCES AND NOTES

1. P. Friedlingstein *et al*., *Earth Syst. Sci. Data* **12**, 3269–3340 (2020).
2. B. Poulter *et al*., *Nature* **509**, 600–603 (2014).
3. A. Ahlström *et al*., *Science* **348**, 895–899 (2015).
4. M. Jung *et al*., *Nature* **541**, 516–520 (2017).
5. V. Humphrey *et al*., *Nature* **592**, 65–69 (2021).
6. S. Piao *et al*., *Glob. Change Biol.* **26**, 300–318 (2020).
7. V. Haverd, A. Ahlström, B. Smith, J. G. Canadell, *Glob. Change Biol.* **23**, 793–800 (2017).
8. R. G. Detmers *et al*., *Geophys. Res. Lett.* **42**, 8177–8184 (2015).
9. X. Ma *et al*., *Sci. Rep.* **6**, 37747 (2016).
10. J. Cleverly *et al*., *Sci. Rep.* **6**, 23113 (2016).
11. Z. Xie *et al*., *Remote Sens. Environ.* **231**, 111270 (2019).
12. A. Bastos *et al*., *Global Biogeochem. Cycles* **34**, e2019GB006393 (2020).
13. L. Teckentrup *et al*., *Biogeosciences* **18**, 5639–5668 (2021).
14. P. M. Cox, C. Huntingford, M. S. Williamson, *Nature* **553**, 319–322 (2018).
15. S. Wenzel, P. M. Cox, V. Eyring, P. Friedlingstein, *Nature* **538**, 499–501 (2016).
16. D. L. Hoover, A. A. Pfennigwerth, M. C. Duniway, *J. Ecol.* **109**, 3280–3294 (2021).
17. N. MacBean *et al*., *Environ. Res. Lett.* **16**, 094023 (2021).
18. G. Tramontana *et al*., *Biogeosciences* **13**, 4291–4313 (2016).
19. P. Bodesheim, M. Jung, F. Gans, M. D. Mahecha, M. Reichstein, *Earth Syst. Sci. Data* **10**, 1327–1365 (2018).
20. M. Jung *et al*., *Biogeosciences* **17**, 1343–1365 (2020).
21. S. Sippel *et al*., *Curr. Clim. Change Rep.* **4**, 266–286 (2018).
22. J. Beringer *et al*., *Biogeosciences* **13**, 5895–5916 (2016).
23. J. Cleverly *et al*., *Environ. Res. Lett.* **14**, 095004 (2019).
24. P. J. Sellers, D. S. Schimel, B. Moore3rd, J. Liu, A. Eldering, *Proc. Natl. Acad. Sci. U.S.A.* **115**, 7860–7868 (2018).
25. P. I. Palmer *et al*., *Nat. Commun.* **10**, 3344 (2019).
26. B. Byrne *et al*., *J. Geophys. Res. Atmos.* **125**, e2019JD032029 (2020).
27. Z. Chen *et al*., *Environ. Res. Lett.* **16**, 054041 (2021).
28. Y. Villalobos, P. Rayner, S. Thomas, J. Silver, *Atmos. Chem. Phys.* **20**, 8473–8500 (2020).
29. S. Sitch *et al*., *Biogeosciences* **12**, 653–679 (2015).
30. H. F. Birch, *Plant Soil* **20**, 43–49 (1964).
31. P. Jarvis *et al*., *Tree Physiol.* **27**, 929–940 (2007).
32. P. Casals, L. Lopez-Sangil, A. Carrara, C. Gimeno, S. Nogués, *Global Biogeochem. Cycles* **25**, GB3012 (2011).
33. A. Kuze *et al*., *Atmos. Meas. Tech.* **9**, 2445–2461 (2016).
34. Materials and methods are available as supplementary materials.
35. A. Butz *et al*., *Geophys. Res. Lett.* **38**, L14812 (2011).
36. T. E. Taylor *et al*., *Earth Syst. Sci. Data* **14**, 325–360 (2022).
37. A. Eldering *et al*., *Science* **358**, eaam5745 (2017).
38. Y. Villalobos *et al*., *Atmos. Chem. Phys. Discuss.* **22**, 8897–8934 (2022).
39. D. Wunch *et al*., *Philos. Trans. R. Soc. London Ser. A* **369**, 2087–2112 (2011).
40. W. Peters *et al*., *Proc. Natl. Acad. Sci. U.S.A.* **104**, 18925–18930 (2007).
41. F. Chevallier *et al*., *J. Geophys. Res.* **115**, D21307 (2010).
42. S. Basu *et al*., *Atmos. Chem. Phys.* **13**, 8695–8717 (2013).
43. S. Besnard *et al*., *PLOS ONE* **14**, e0211510 (2019).
44. T. E. Huxman *et al*., *Oecologia* **141**, 254–268 (2004).
45. F. E. Moyano, S. Manzoni, C. Chenu, *Soil Biol. Biochem.* **59**, 72–85 (2013).
46. W. Borken, E. Matzner, *Glob. Change Biol.* **15**, 808–824 (2009).
47. J. P. Schimel, *Annu. Rev. Ecol. Evol. Syst.* **49**, 409–432 (2018).
48. V. K. Arora *et al*., *Biogeosciences* **17**, 4173–4222 (2020).
49. X. Lian *et al*., *Nat. Rev. Earth Environ.* **2**, 232–250 (2021).
50. A. Butz, RemoTeC full-physics retrieval GOSAT/TANSO-FTS Level 2 bias-corrected XCO2 version 2.4.0 operated at Heidelberg University, RemoTeCv2.4.0, Zenodo (2022); https://doi.org/10.5281/zenodo.5886662.
51. E.-M. Metz, ATMO-IUP-UHEI/MetzEtAl2023: v1.0.0, version 1.0.0, Zenodo (2023); https://doi.org/10.5281/zenodo.7648699.

ACKNOWLEDGMENTS

We gratefully acknowledge the data storage service SDS@hd supported by the Ministry of Science, Research and the Arts Baden-Württemberg (MWK) and the computing resources provided by the DKRZ under project bb1170. E.-M.M. acknowledges a doctoral scholarship from the German National Academic Foundation. We thank the Japanese Aerospace Exploration Agency, the National Institute for Environmental Studies, and the Ministry of Environment for the GOSAT data and their continuous support as part of the Joint Research Agreement. We thank the OCO-2 science team for producing the GOSAT/ACOS L2 XCO2 data. OCO-2 data were produced by the OCO-2 project at the Jet Propulsion Laboratory, California Institute of Technology, and obtained from the OCO-2 data archive maintained at the NASA Goddard Earth Science Data and Information Services Center. CarbonTracker CT2019B results were provided by NOAA ESRL, Boulder, Colorado, USA, from the website at http://carbontracker.noaa.gov. We thank all TRENDY modelers for providing model output as part of the TRENDY v9 ensemble. R.S. thanks the Météo-France/DSI supercomputing center, which provided computing time for performing TRENDY simulations. D.S.G. acknowledges support from the ANR CLAND Convergence Institute. This study has greatly benefited from discussions with C. Frankenberg. **Funding:** Funding was provided by the German Research Foundation (DFG) through grants BU2599/1-1 and INST 35/1503-1 FUGG and by the Darwin and Wollongong TCCON stations through ARC grants DP160100598, LE0668470, DP140101552, DP110103118, and DP0879468 and Darwin through NASA grants NAG5-12247 and NNG05-GD07G. S.Z. was supported by EU H2020 grant 821003, 4C; S.B. was supported by NASA grant 80NSSC20K0818; and R.S. was supported by EU H2020 CRESCENDO (641816) and ESM2025 (101003536). **Author contributions:** A.B., S.N.V., and E.-M.M. were involved in conceptualization and methodology. E.-M.M. conducted the formal analysis and the visualization under the supervision of A.B. and S.N.V. A.B., S.N.V., E.-M.M., M.J., and S.B. wrote the original draft. S.B. performed the dedicated TM5-4DVAR runs. S.S., V.K.A., P.R.B., P.F., D.S.G., A.K.J., E.K., D.L., J.E.M.S.N., B.P., R.S., H.T., A.W., W.Y., X.Y., and S.Z. provided TRENDY data. N.M.D. and D.W.T.G. provided TCCON data. All authors contributed to the editing and review of the manuscript. **Competing interests:** The authors declare that they have no competing interests. **Data and materials availability:** GOSAT/RemoTeC2.4.0 XCO2 data can be obtained from Zenodo (*50*) (last access: 2022-02-25). GOSAT/ACOS data are available at https://oco2.gesdisc.eosdis.nasa.gov/data/GOSAT_TANSO_Level2/ACOS_L2_Lite_FP.9r/ (last access: 2020-07-28). OCO-2 data are available at https://disc.gsfc.nasa.gov/datasets/OCO2_L2_Lite_FP_10r/summary (last access: 2020-11-01). TCCON data can be downloaded at https://data.caltech.edu/records/269 (last access: 2022-02-25). CarbonTracker CT2019B CO2 fluxes and concentrations can be downloaded from https://gml.noaa.gov/aftp/products/carbontracker/co2/CT2019B/fluxes/monthly/ (last access: 2021-02-19) and https://gml.noaa.gov/aftp/products/carbontracker/co2/CT2019B/molefractions/co2_total_monthly/ (last access: 2022-02-25), respectively. CAMS concentrations and fluxes can be found at https://ads.atmosphere.copernicus.eu/cdsapp#!/dataset/cams-global-greenhouse-gas-inversion (last access: 2021-10-07). GFAS emissions records are available at https://apps.ecmwf.int/datasets/data/cams-gfas/ (last access: 2020-11-13). CAMS and GFAS data were generated using Copernicus Atmosphere Service Information [2021], and neither the European Commission nor the European Centre for Medium-Range Weather Forecasts (ECMWF) is responsible for any use that may be made of the information it contains. GFED fire emissions are available at https://www.geo.vu.nl/~gwerf/GFED/GFED4/ (last access: 2020-07-10). FINN data were retrieved from the American National Center for Atmospheric Research https://www2.acom.ucar.edu/modeling/finn-fire-inventory-ncar (last access: 2020-11-18). The MIP data used in this work can be downloaded from https://www.gml.noaa.gov/ccgg/OCO2_v10mip/ (last access: 2022-11-06). ERA5-land data records contain modified Copernicus Atmosphere Service Information [2021] available at the Climate Data Store https://cds.climate.copernicus.eu/cdsapp#!/dataset/reanalysis-era5-land-monthly-means (last access: 2021-12-20). This work used eddy covariance data collected by the TERN-OzFlux facility. OzFlux acknowledges the financial support of the Australian Federal Government via the National Collaborative Research Infrastructure Scheme and the Education Investment Fund. OzFlux data are available at https://data.ozflux.org.au (last access: 2023-01-20). TRENDYv9 model output and FLUXCOM products are available at https://sites.exeter.ac.uk/trendy and http://fluxcom.org/CF-Download/, respectively. Data S1 to S3 in the supplementary materials contain monthly TRENDY and FLUXCOM data used in this study. Monthly TM5-4DVAR data are available in data S1 and S4. The code used in this study is available at Zenodo (*51*) or GitHub (https://github.com/ATMO-IUP-UHEI/MetzEtAl2023).

SUPPLEMENTARY MATERIALS

science.org/doi/10.1126/science.add7833
Materials and Methods
Figs. S1 to S12
Tables S1 and S2
References (*52*–*132*)
Data S1 to S4

Submitted 4 July 2022; accepted 6 March 2023
10.1126/science.add7833

Soil respiration–driven CO_2 pulses dominate Australia's flux variability

Eva-Marie Metz, Sanam N. Vardag, Sourish Basu, Martin Jung, Bernhard Ahrens, Tarek El-Madany, Stephen Sitch, Vivek K. Arora, Peter R. Briggs, Pierre Friedlingstein, Daniel S. Goll, Atul K. Jain, Etsushi Kato, Danica Lombardozzi, Julia E. M. S. Nabel, Benjamin Poulter, Roland Sfrian, Hanqin Tian, Andrew Wiltshire, Wenping Yuan, Xu Yue, Snke Zaehle, Nicholas M. Deutscher, David W. T. Griffith, and Andr Butz

Science, **379** (6639), .
DOI: 10.1126/science.add7833

The exhalation of drylands

Semi-arid regions cause much of the interannual variability in global atmospheric carbon dioxide concentration because of seasonal fluctuations in water availability. Metz *et al*. found that recurrent carbon dioxide pulses occur at the end of the dry season over Australia, an effect that they attribute to enhanced soil respiration preceding photosynthetic uptake in semi-arid regions. The magnitudes of these pulses are two to three times larger than previous studies have inferred based on in situ measurements. —HJS